Electronic Supplementary Material (ESI) for Nanoscale.

Supporting Information

Promoting CO_2 Electroreduction on CuO Nanowire with a Hydrophobic Nafion Overlayer

Mang Wang, Lili Wan, Jingshan Luo*

Institute of Photoelectronic Thin Film Devices and Technology, Key Laboratory of Photoelectronic Thin Film Devices and Technology of Tianjin, Ministry of Education Engineering Research Center of Thin Film Photoelectronic Technology, Nankai University, Tianjin 300350, China

*Correspondence to: jingshan.luo@nankai.edu.cn (J. Luo)

Reagents

Reagents including KOH (99.999%, metals basis), nafion-117 solution (5%), $KHCO_3$(99.995%) were purchased from Aladdin chemical company and used without further purification. HCl, H_2SO_4 and ethanol were analytical pure and purchased from SHIJIKEBO Co., Ltd. Cu mesh was purchased from Suzhou jiashide metal foam Co., Ltd. Ultrapure water was used in the whole experiments (Sartorius-mini plus UV, 18.2 MΩ cm^{-1}). CO_2 (99.999%) and N_2 (99.999%) gases were purchased from Air Liquid Co., Ltd.

Physical and chemical characterizations

Powder X-ray diffraction (PXRD) patterns were obtained with a Rigaku SmartLab 9.0 using Cu Kα radiation (λ = 1.54056 Å), and the data were collected in Bragg-Brettano mode in the 2θ range from 10° to 80° at a scan rate of 5° min^{-1}. Scanning electron microscopic (SEM) images were captured on a JSM-7800F field-emission scanning electron microscope operated at an acceleration voltage of 20 kV. Transmission electron microscopy (TEM) images were collected on a FEI Tecnai G2 F30 S-TWIN transmission electron microscope with an acceleration voltage of 300 kV. X-ray photoelectron spectroscopy (XPS) spectra were taken on a ThermoFisher ESCALAB^{TM} 250Xi surface analysis system using a monochromatized Al Kα small-spot source, and the corresponding BEs were calibrated by referencing the C 1s to 284.8 eV. Contact angle measurements and the slow motion video were made on a Contact Angle Meter (SDC-80, DONGGUAN SHENGDING PRECISION INSTRUMENT Co., LTD) with a drop of aqueous 0.1 M $KHCO_3$ solution.

Electrochemical measurements

All electrochemical measurements were carried out in a customized gastight two-compartment electrochemical cell with a three-electrode configuration. Typically, the R-CuO-Nafion or R-CuO (0.5*0.5 cm^2) were used as working electrodes and mounted in the cathodic compartment, and a leakless Ag/AgCl reference electrode (Saturated KCl, Tjaida) was used to monitor the potential on the work electrodes. A Ti@IrO_2 electrode was used as counter electrode and mounted in the anodic compartment. An anion-exchange membrane (Selemion AMVN, AGC Inc.) was used to separate the cathodic and anodic compartments to eliminate the oxidation of the liquid products at the anode surface. The volumes of catholyte and anolyte were 8 mL and 7 mL, respectively. The headspace of the cathodic compartment was about 6 mL. CO_2-saturated 0.1 M $KHCO_3$ aqueous solution (pH 6.8) was used as the electrolyte and CO_2 gas was introduced into catholyte at a flow rate of 10 standard cubic centimeters per minute (SCCM) during the electrocatalytic reaction. The electrolyte was stirred by a stir bar during the electrolysis. The cell was connected to the potentiostat (Autolab) and chronoamperometry experiments were performed for 40 minutes at different potentials for performance tests. The gaseous products were detected by a gas chromatograph (GC, Thermo Fisher) equipped with a thermal conductivity detector (TCD) for

hydrogen (H_2) and two flame ionization detectors (FID) for CO, methane (CH_4), ethane (C_2H_6) and ethylene (C_2H_4). The peak identification and peak area were calibrated using standard calibration gas with known concentration of H_2, CO, CH_4, C_2H_6 and C_2H_4 mixed with Ar from a commercial supplier (Dalian GuangMing Special Gas Products Co., Ltd.). After electrolysis, 900 μL of the catholyte was acidized with 100 μL of 4.5 M H_2SO_4 and the liquid products were quantified with high performance liquid chromatograph (HPLC, Agilent 1260 Infinity). While formate and acetate were detected using variable wavelength detector (VWD, 210 nm), ethanol, acetone and isopropanol were detected by refractive index detector (RID). The Potential (E) was converted to the RHE reference electrode using the following equation:

$$E\ (vs.\ RHE) = E\ (vs.\ Ag/AgCl) + 0.1976 + 0.059*pH$$

Preparation of Ti@IrO_2 electrode

Ti@IrO_2 electrode was prepared according to previous literature.[1] Briefly, 50 μL of 0.2 M H_2IrCl_6 in isopropanol was drop cast onto one side of Ti foil (2*1*0.1 cm) etched by boiling oxalic acid, after drying at 70 °C for 10 min, the other side of the foil was treated with the same process. Then, the foil was calcined at 500 °C for 10 min in a muffle furnace. Finally, the Ti@IrO_2 electrode was obtained after repeating the above process three times.

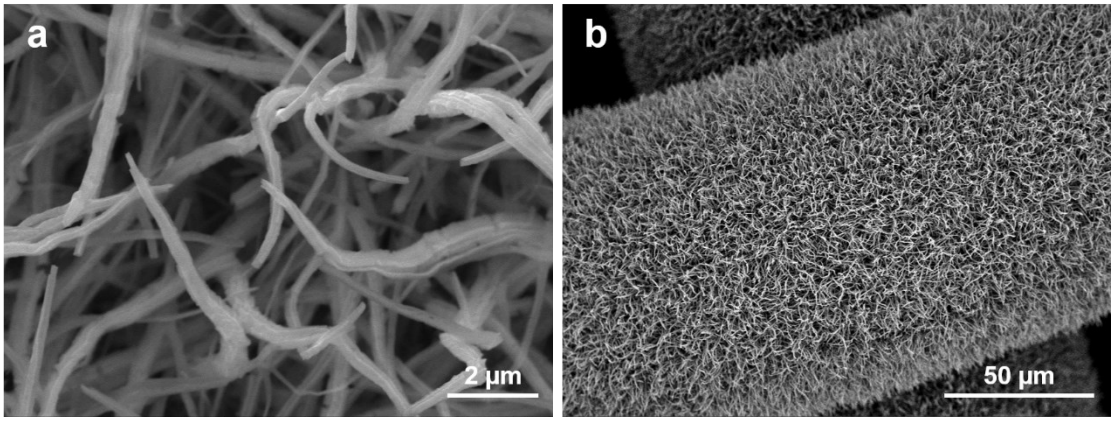

Figure. S1 SEM images of the CuO-Nafion-60 nanowire electrode.

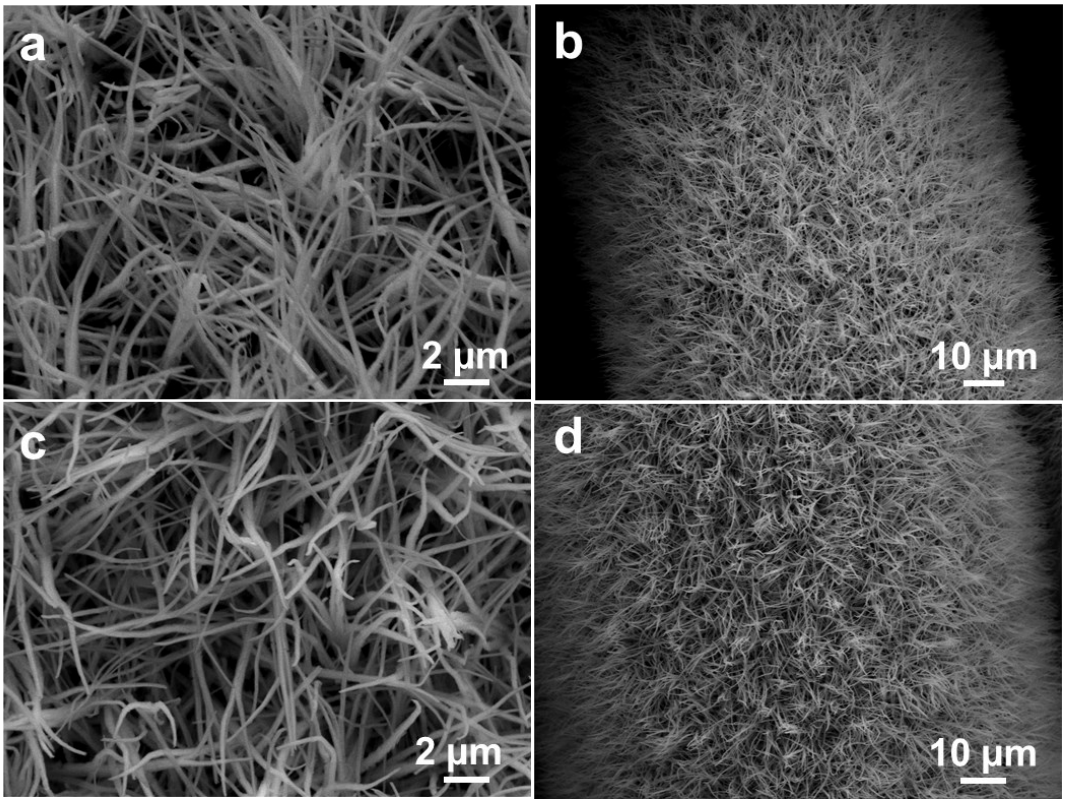

Figure. S2 SEM images of the CuO-Nafion-20 (a,b) and CuO-Nafion-180 (c,d) nanowire electrode.

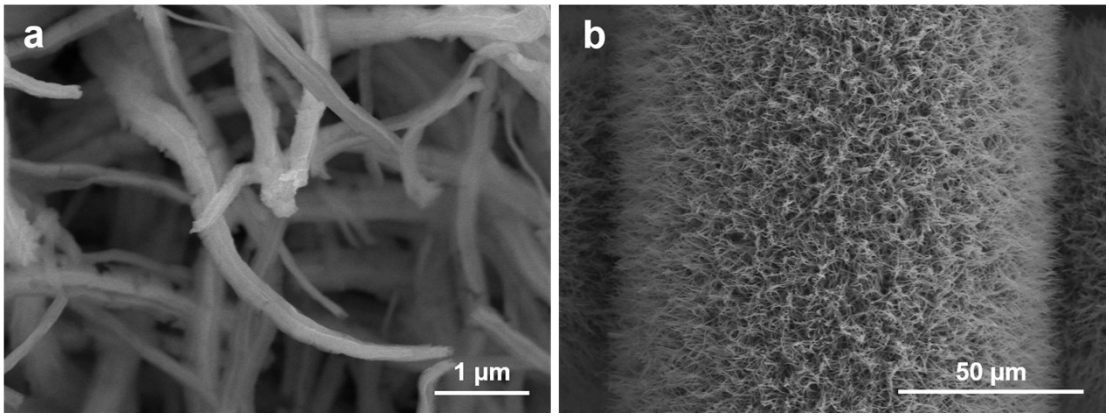

Figure. S3 SEM images of the CuO nanowire electrode.

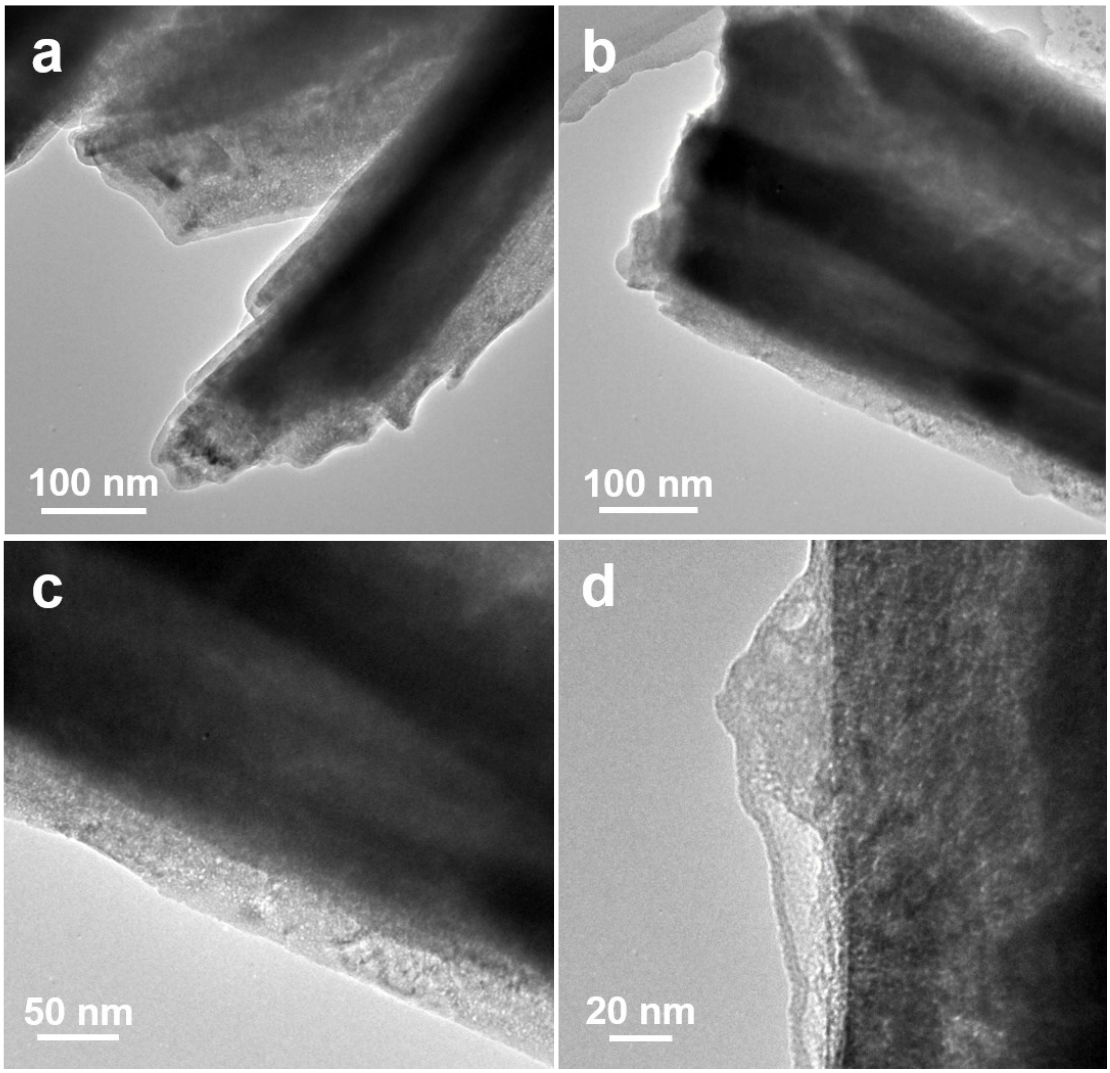

Figure. S4 TEM images of the CuO-Nafion-60 nanowire.

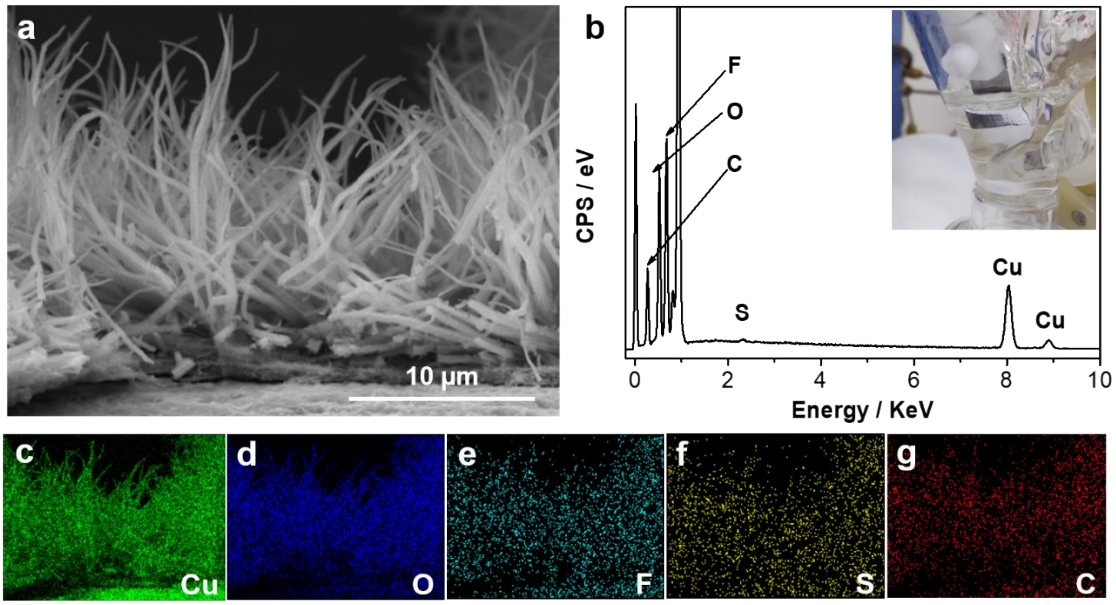

Figure. S5 Cross-section SEM image (a) and the EDS spectrum (b) of CuO-Nafion-60 nanoforest, as well as the corresponding elemental mappings (c-g). Inset in b is a photo of the hydrophobic electrode immersing in the electrolyte.

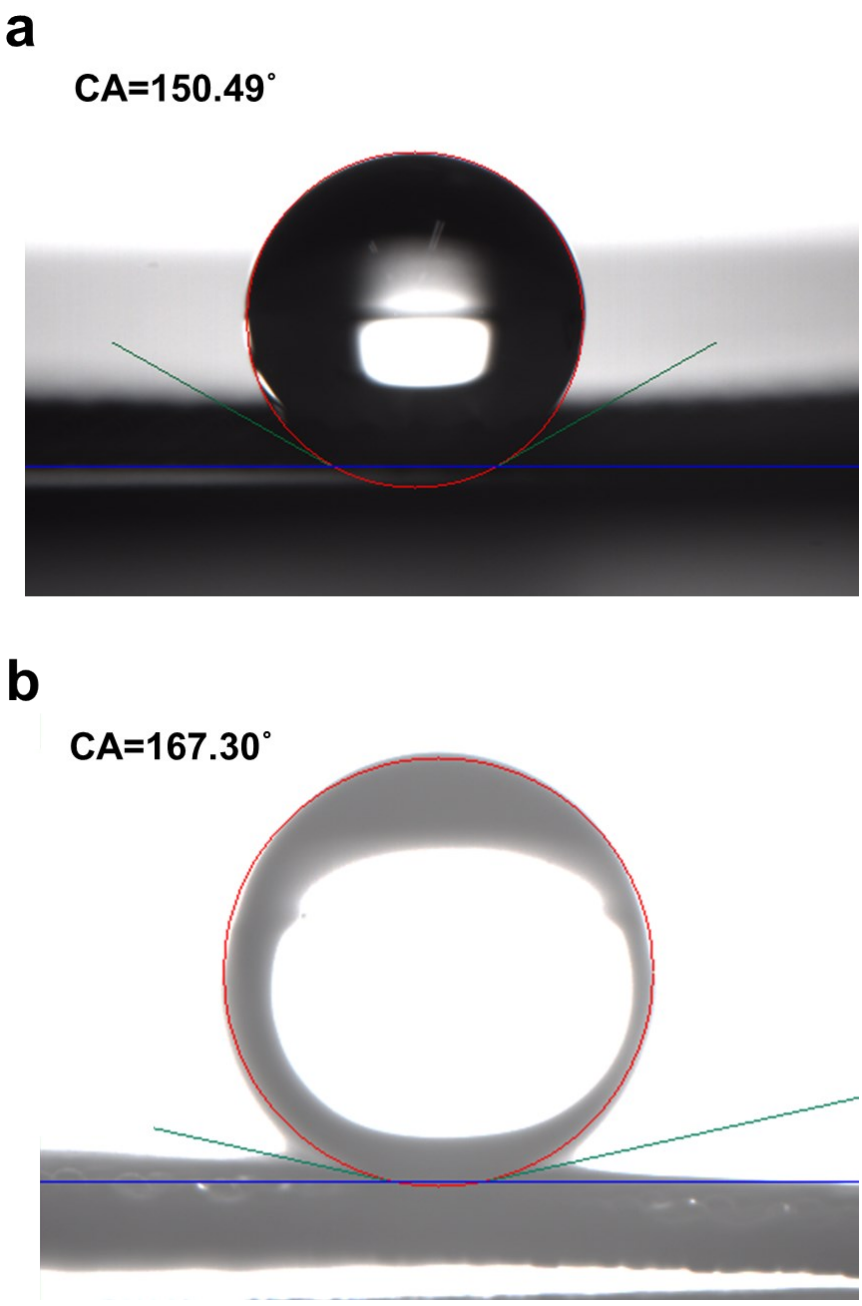

Figure. S6 Contact angle of 0.1 M $KHCO_3$ aqueous solution on the CuO-Nafion-20 (a) and CuO-Nafion-180 (b) electrode, respectively.

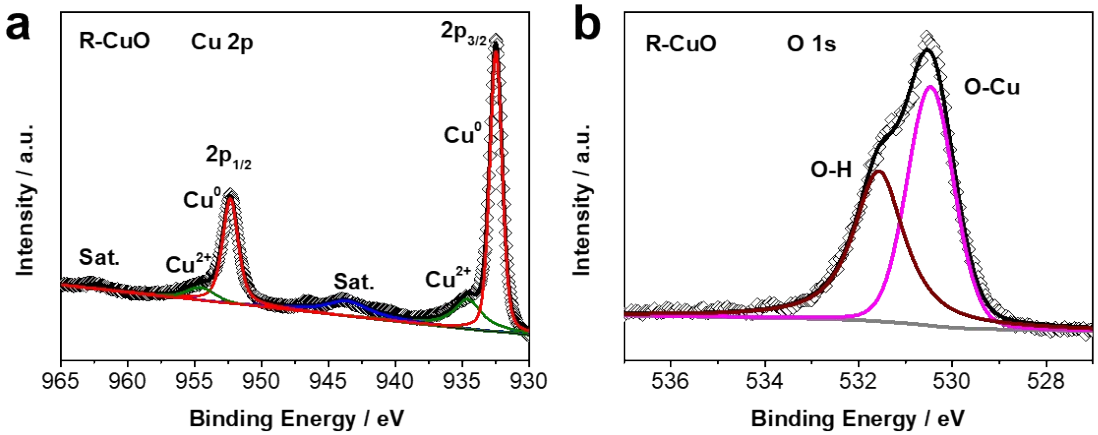

Figure. S7 XPS spectra of Cu 2p and O 1s of the R-CuO electrode.

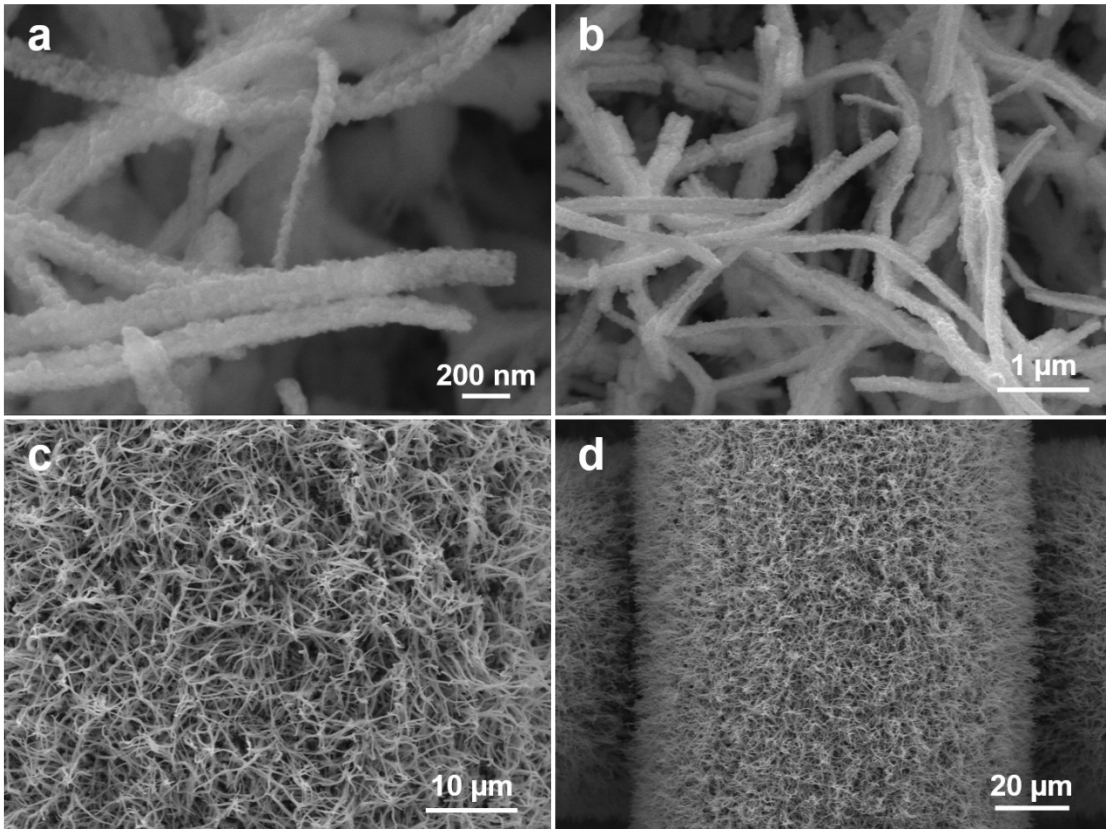

Figure. S8 SEM images of the R-CuO-Nafion-60 nanowire electrode.

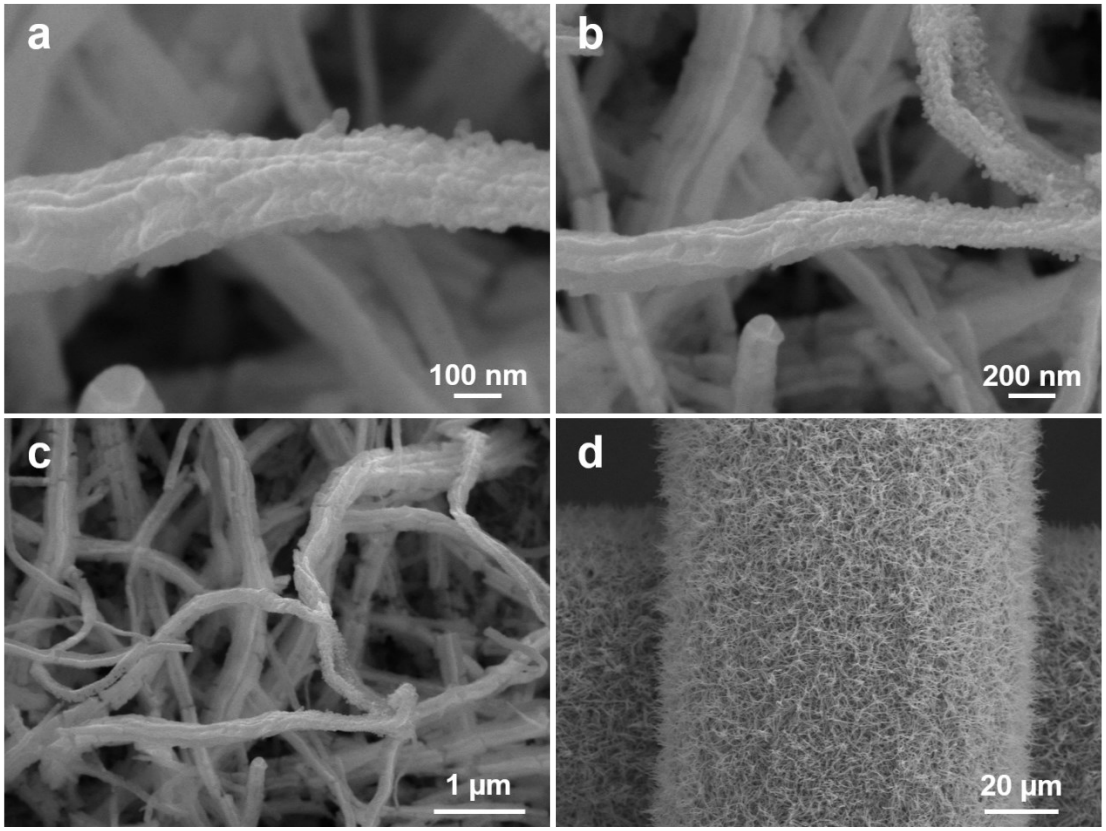

Figure. S9 SEM images of the R-CuO nanowire electrode.

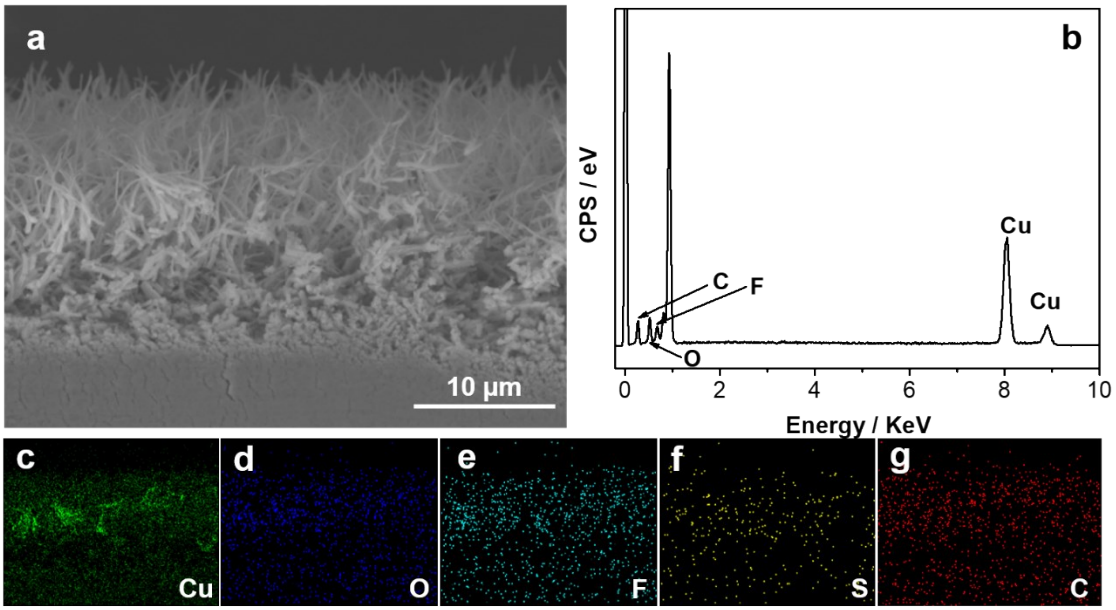

Figure. S10 Cross-section SEM image (a) and the EDS spectrum (b) of R-CuO-Nafion nanoforest, as well as the corresponding elemental mappings (c-g).

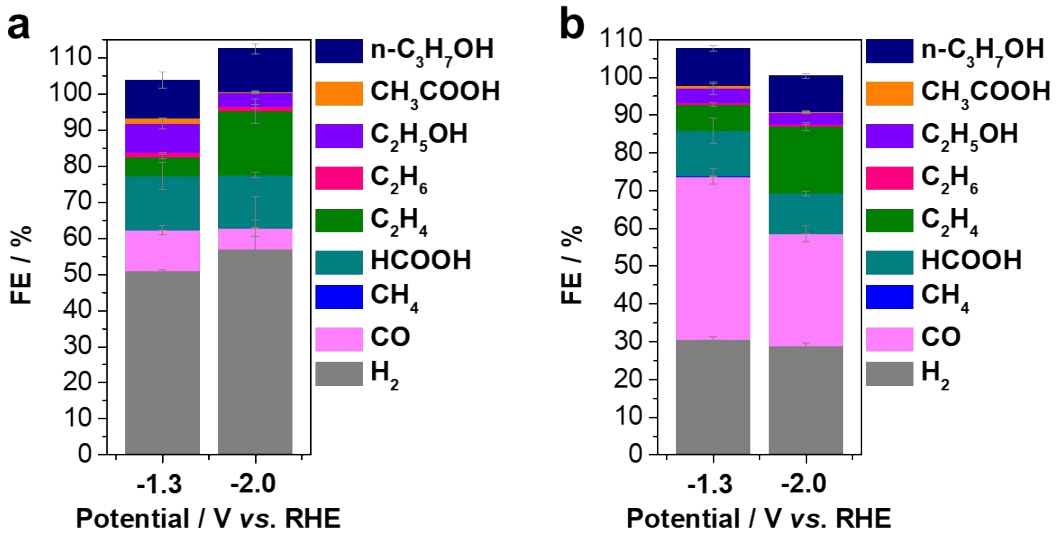

Figure. S11 Products distribution on (a) R-CuO-Nafion-20 and (b) R-CuO-Nafion-180 nanowire electrodes under different working potentials.

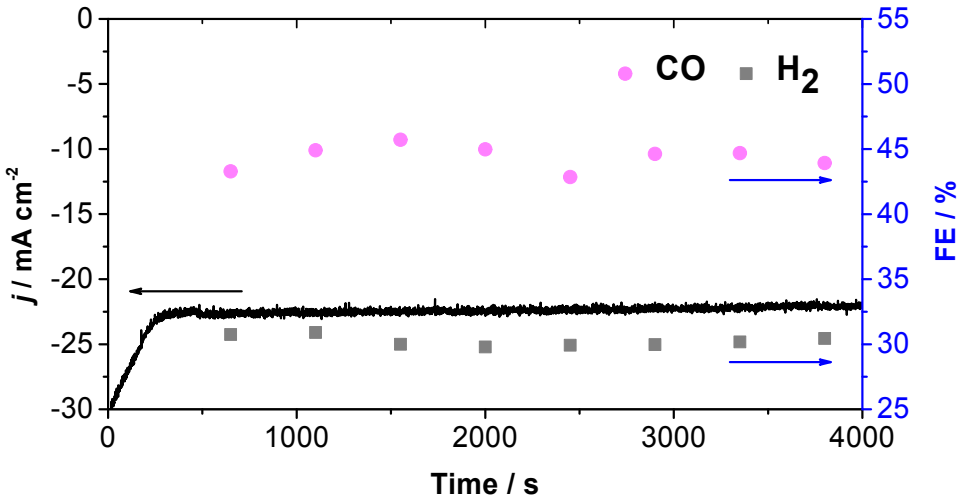

Figure. S12 Stability test of R-CuO-Nafion-180 electrode at -1.3 V *vs*. RHE.

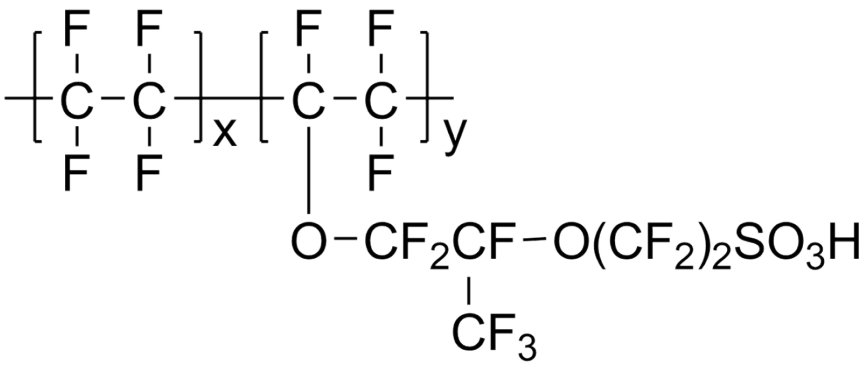

Figure. S13 Molecular structure of Nafion.

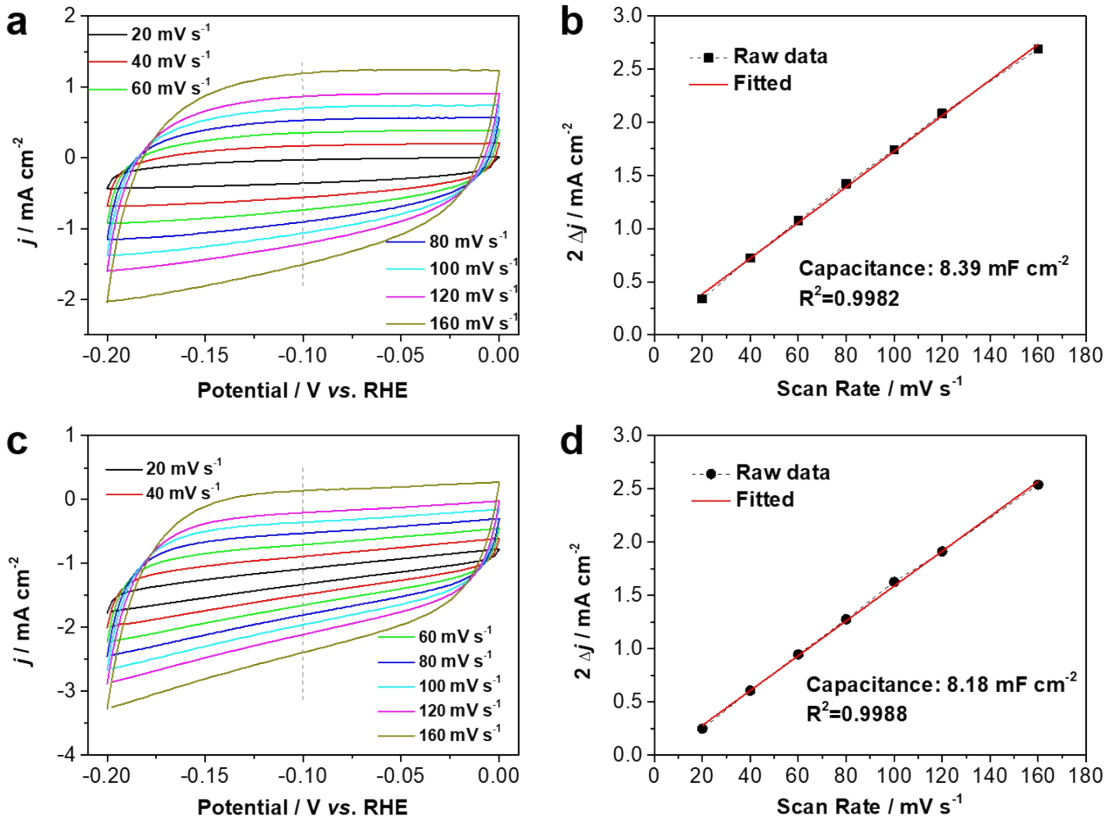

Figure. **S14** Double layer capacitance measurements for determining electrochemically active surface area (ECSA) of the electrodes in 0.1 M $KHCO_3$ (Ar saturated). Cyclic voltammograms of the R-CuO (a) and R-CuO-Nafion electrode (c) in a non-Faradaic region at different scan rates. The double layer capacitance (C_{dl}) of the R-CuO (b) and R-CuO-Nafion electrode (d). The C_{dl} was calculated by plotting half of the difference of the anodic and cathodic currents (i_a - i_c) at -0.1 V *vs*. RHE against scan rate.

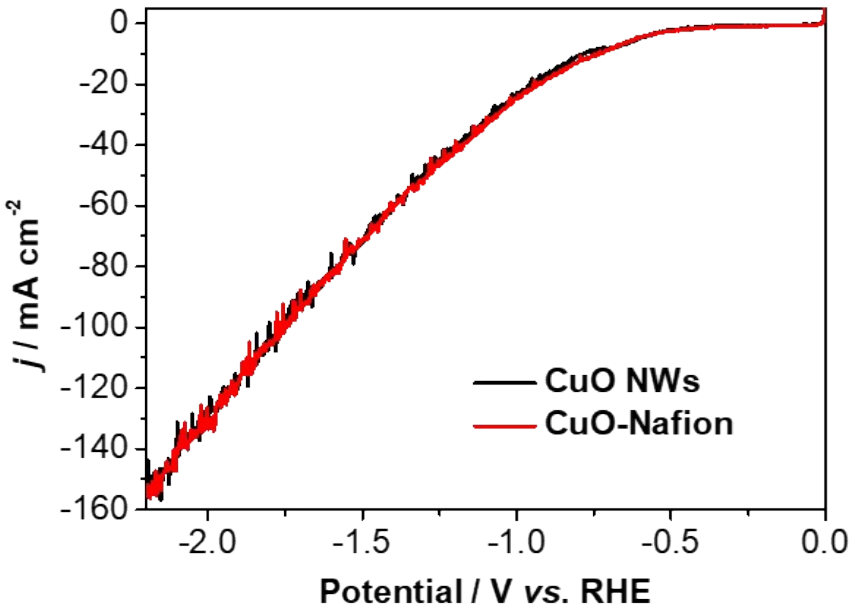

Figure. **S15** Linear sweep voltammograms of the R-CuO-Nafion and R-CuO electrodes in CO_2-saturated 0.1 M $KHCO_3$ electrolyte at a scan rate of 20 mV/s (without stirring).

Table S1. Faradaic efficiency of all detectable products on R-CuO electrode at different applied potentials.

E *vs.* RHE (V)	H_2	CO	CH_4	$HCOO^-$	C_2H_4	C_2H_6	C_2H_5OH	CH_3COO^-	$(CH_3)_2CO$	n-C_3H_7OH
-1.3	41.32	8.72	0.01	16.33	11.81	1.86	7.19	0.24	1.70	6.56
-1.4	41.62	7.41	0.02	14.57	13.25	1.86	8.01	0.29	2.73	7.49
-1.5	40.99	6.79	0.04	14.4	15.68	1.50	7.11	0.30	2.41	6.89
-1.6	39.79	5.82	0.04	12.09	17.87	1.52	7.74	0.32	2.00	9.00
-1.7	38.58	4.62	0.07	10.88	19.02	1.38	13.33	0.28	2.61	7.77
-1.8	40.89	3.78	0.14	8.34	23.19	1.55	11.79	0.37	2.17	6.73
-1.9	41.24	3.55	0.07	9.02	21.23	1.80	11.47	0.35	1.87	6.54
-2.0	40.26	3.13	0.10	8.15	21.88	1.56	13.13	0.40	1.74	6.54

Table S2. Faradaic efficiency of all detectable products on R-CuO-Nafion electrode at different applied potentials.

E *vs.* RHE (V)	H_2	CO	CH_4	$HCOO^-$	C_2H_4	C_2H_6	C_2H_5OH	CH_3COO^-	$(CH_3)_2CO$	n-C_3H_7OH
-1.3	30.28	33.00	/	15.82	9.39	0.57	6.48	0.52	1.29	5.98
-1.4	39.17	20.10	0.01	14.70	11.53	1.39	6.00	0.67	1.80	6.28
-1.5	31.16	26.66	0.01	13.68	12.62	0.56	7.76	0.52	1.61	5.79
-1.6	34.18	19.43	0.02	14.35	14.67	0.71	5.56	0.49	1.28	6.11
-1.7	29.78	23.11	0.03	15.86	15.49	0.62	10.45	0.65	2.04	7.21
-1.8	33.39	17.33	0.04	11.88	18.41	0.67	7.70	0.51	1.36	6.28
-1.9	30.37	21.41	0.05	9.30	19.87	0.58	9.80	0.56	1.19	5.54
-2.0	30.24	18.59	0.07	9.71	20.90	0.62	10.87	0.48	1.41	6.46

Table. S3 Overview of the performances of CuO nanostructure electrodes for the reduction of CO_2 to CO

Catalyst	**Potential V vs. RHE**	**Electrolyte**	**Faradic Efficiency / %**	**Current density / $mAcm^{-2}$**	**Reference**
R-CuO-Nafion	-1.3	0.1 M $KHCO_3$	43.15	~ -22.5	**This work**
Cu NW-BTEAC	-0.8	0.1 M $KHCO_3$	45.8	~ -7	2
PTFE-Cu NW	-0.7	0.1 M $KHCO_3$	~38	~ -2.5	3
CuO NW	-1.1	0.1 M $KHCO_3$	7.6	~ -4.5	4
ECR-Cu NW	-0.4	0.1 M $KHCO_3$	61.8	~ -1	5
CuO NW	-0.6	0.1 M $KHCO_3$	19.1	-2.2	6
Cu-X	-0.8	0.1 M $KHCO_3$	78	-13.2	7
CuO NW	-0.6	0.1 M $NaHCO_3$	36	~ -0.6	8
CuO NW	-0.6	0.1 M $KHCO_3$	50	~ -0.6	9
OD-Cu-1 NW	-1.0	0.1 M $KHCO_3$	~ 18	~ -6	10

Reference

1. M. Wang, Q. Zhang, Q. Xie, L. Wan, Y. Zhao, X. Zhang and J. Luo, Selective electrochemical reduction of carbon dioxide to ethylene on a copper hydroxide nitrate nanostructure electrode. Nanoscale, 2020, 12 (32), 17013-17019.

2. Y. Zhong, Y. Xu, J. Ma, C. Wang, S. Sheng, C. Cheng, M. Li, L. Han, L. Zhou, Z. Cai, Y. Kuang, Z. Liang and X. Sun, An artificial electrode/electrolyte Interface for CO_2 electroreduction by cation surfactants self-assembly, Angew. Chem. Int. Ed. 2020, 59, 19095-19101.

3. Z. Cai, Y. Zhang, Y. Zhao, Y. Wu, W. Xu, X. Wen, Y. Zhong, Y. Zhang, W. Liu, H. Wang, Y. Kuang and X. Sun, Selectivity regulation of CO_2 electroreduction through contact interface engineering on superwetting Cu nanoarray electrodes, Nano Res. 2019, 12, 345-349.

4. M. Ma, K. Djanashvili and W. A. Smith, Controllable Hydrocarbon Formation from the Electrochemical Reduction of CO_2 over Cu Nanowire Arrays. Angew. Chem. Int. Ed. Engl. 2016, 55 (23), 6680-6684.

5. D. Raciti, K. J. Livi and C. Wang, Highly dense Cu nanowires for low-overpotential CO 2 reduction, Nano Lett. 2015, 15, 6829-6835.

6. D. Ren, J. G., L. Pan, Z. Wang, J. Luo, S. M. Zakeeruddin, A. Hagfeldt and M. Grätzel, Atomic Layer Deposition of ZnO on CuO Enables Selective and Efficient Electroreduction of Carbon Dioxide to Liquid Fuels. Angew. Chem. Int. Ed. 2019, 58 (42), 15036-15040.

7. P. Huang, J. Chen, P. Deng, F. Yang, J. Pan, K. Qi, H. Liu and B. Xia, Grain refinement of self-supported copper electrode by multiple-redox treatment for enhanced carbon dioxide electroreduction towards carbon monoxide generation, J. Catal. 2020, 381, 608-614.

8. M. Schreier, F. Héroguel, L. Steier, S. Ahmad, J. S. Luterbacher, M. T. Mayer, J. Luo and M. Grätzel, Solar conversion of CO_2 to CO using earth-abundant electrocatalysts prepared by atomic layer modification of CuO, Nat. Energy, 2017, 2, 17087-17096.

9. M. Ma, K. Djanashvili and W. A. Smith, Selective electrochemical reduction of CO_2 to CO on CuO-derived Cu nanowires, Phys. Chem. Chem. Phys., 2015, 17, 20861-20867.

10. F. Yang, P. Deng, Q. Wang, J. Zhu, Y. Yan, L. Zhou, K. Qi, H. Liu, H. S. Park and B. Xia, Metal-organic framework-derived cupric oxide polycrystalline nanowires for selective carbon dioxide electroreduction to C_2 valuables, J. Mater. Chem. A, 2020, 8, 12418-12423.